Eur. Phys. J. D **4**, 343–352 (1998)

THE EUROPEAN PHYSICAL JOURNAL D

Plasmon response in K, Na and Li clusters: systematics using the separable random-phase-approximation with pseudo-Hamiltonians

W. Kleinig[1,2], V.O. Nesterenko[1], P.-G. Reinhard[3,a], and Ll. Serra[4]

[1] Bogoliubov Laboratory of Theoretical Physics, Joint Institute for Nuclear Research, 141980 Dubna, Moscow region, Russia
[2] Technische Universität Dresden, Institut für Analysis, 01062 Dresden, Germany
[3] Institut für Theoretische Physik, Universität Erlangen, Staudtstrasse 7, 91058 Erlangen, Germany
[4] Departament de Física Universitat de les Illes Balears, 07071 Palma de Mallorca, Spain

Received: 22 April 1998 / Accepted: 24 July 1998

Abstract. The systematics of the plasmon response in spherical K, Na and Li clusters in a wide size region ($8 \leq N \leq 440$) is studied. Two simplifying approximations whose validity has been established previously are considered: (a) a separable approach to the random-phase-approximation, involving an expansion of the residual interaction into a sum of separable terms, (b) the electron-ion interaction is modeled within the pseudo-Hamiltonian jellium model (PHJM) including nonlocal effects by means of realistic atomic pseudoHamiltonians. In cases where nonlocal effects turn out to be negligible, the Structure Averaged Jellium Model (SAJM) has been used. The leading role of Landau damping in forming the plasmon width in medium and large clusters is demonstrated. Good agreement with available experimental data is achieved for K, Na (using the SAJM) and small Li clusters (invoking the PHJM). The trends for peak position and width are generally well reproduced, even up to details of the Landau fragmentation in several clusters. Less good agreement, however, is found for large Li clusters. The possible reasons of the discrepancy are discussed.

PACS. 36.40.Cg Electronic and magnetic properties of clusters – 36.40.Gk Plasma and collective effects in clusters – 36.40.Vz Optical properties of clusters – 36.40.Wa Charged clusters

1 Introduction

Optical response has been for a long time one of the main tools to investigate the properties of metal clusters. See reference [1] for early experiments and references [2,3] for early theoretical explanations. Remarkable progress in experimental photoabsorption techniques and continued studies on the subject have accumulated in the meantime, producing an important amount of information covering the range from small ($N \sim 8$) up to medium-heavy ($N \sim 500$) clusters for a variety of materials, see, *e.g.*, references [4–10]. The experimental development was, of course, accompanied by equally intense theoretical studies at various levels of approaches. Among the studies involving the detailed microscopic description of the electronic response one has: time-dependent local-density-approximation (TDLDA), or equivalently random-phase-approximation (RPA), with the steep [2,3,11,12] and soft [13–16] jellium model; TDLDA with the pseudo-Hamiltonian (or pseudopotential) jellium model (PHJM) which accounts for nonlocal ionic effects in an spherically averaged fashion [17–23]; TDLDA with a structure averaged jellium model (SAJM) which incorporates volume averaged local pseudopotentials and structure effects [24–26]; TDLDA in real time with realistic ionic pseudopotentials [27,28]; fully microscopic RPA with explicit treatment of exchange and correlations [29,30]; shell-model theory [31]; and even quantum chemical *ab-initio* calculations [32]. For recent reviews and a more complete list of citations see [33–36].

The aim of this paper is a systematic theoretical investigation of the dipole optical response of three different types of alkali-metal clusters, namely K, Na and Li. These three metals are distinguished not only by different values of their Wigner-Seitz radii (in atomic units $r_s(\mathrm{K}) = 5$, $r_s(\mathrm{Na}) = 3.96$, and $r_s(\mathrm{Li}) = 3.25$) but also, and more importantly, by a different influence of the ionic structure on the cluster's dynamical properties. Motivated by the available experimental data, clusters in the size range $8 \leq N_e \leq 440$ (where N_e is the number of valence electrons) will be considered. Thereby we will pay particular attention to the evolution of the Landau fragmentation with cluster size and with varying material, as well as the general trends of peak energies and widths. A strong motivation for this survey comes also from the appearance

[a] e-mail: reinhard@theorie2.physik.uni-erlangen.de

of new photoabsorption data for small Li clusters [10] which allow us to further analyze the impact of the ionic-core structure in these clusters.

As theoretical tools for this survey, we employ TDLDA calculations, linearized for the case of small oscillations. This is often also called Random-Phase Approximation (RPA), a name which we will use from now on. The RPA calculations are performed on the Kohn-Sham ground state of the electronic cloud and they employ consistently the same energy-density functional. Another essential input is the description of the ionic background. We will model it using the PHJM and the SAJM, where comparison of both allows to deduce the particular ionic effects. The SAJM includes ionic structure effects in an averaged manner [24]. It was designed predominantly to compute properly the systematics of ground state properties in all sorts of metals, as *e.g.* cohesive energy, surface tension, or ground state deformation. The crucial ingredient for the plasmon response is the use of a pseudopotential-folded jellium background whose softer surface places the plasmon position quite correctly [25] (we ought to mention, however, that this effect of a soft jellium surface was advocated earlier in [38]). The SAJM provides fairly accurate plasmon properties for K and Na clusters, as will be shown in Section 3. More elaborate is the PHJM which consists essentially in the spherical average of a realistic atomic pseudo-Hamiltonian [37], designed to take into account nonlocal effects of core electrons on valence electrons in the isolated atom. This average produces a global cluster pseudo-Hamiltonian with a similar structure of the atomic one and thus retains its nonlocal features. In particular, a radial-dependent effective mass and angular-momentum-dependent potential for each Kohn-Sham orbital are obtained. The model is then also capable of describing Li clusters where nonlocal effects become crucial.

In fact, both SAJM and PHJM are closely related. The SAJM can be derived from ionic structure models if *local* pseudopotentials are employed, and the PHJM follows a similar strategy but is more general in that it allows also for *nonlocal* pseudopotentials. Thus comparing SAJM and PHJM we easily judge on the possibility of a purely local treatment in contrast to the need for nonlocal models. Obviously, in modeling the PHJM an essential input is the parameterization of the atomic pseudo-Hamiltonian. We use in the present paper a new parameterization of the Li pseudo-Hamiltonian as recently proposed in [22]. In the bulk limit for lithium, the associated PHJM effective electron mass (see the definition in Eq. (34) of [18]) becomes $m_e^*/m_e \sim 1.2$, which is considerably less than the value $m_e^*/m_e \sim 1.5$ of PHJM calculations based on a previous parameterization [17]. The new value is more realistic, since it reproduces the result of more elaborated pseudopotentials (see Tab. 1 of [23]). It is interesting to look at the consequences of this new parameterization on the plasmon peak position in Li clusters.

The RPA treatment is much simplified when invoking an expansion of the residual interaction into a sum of separable terms, leading to a "separable RPA" (SRPA). It was shown earlier that such an expansion converges quickly (within 4−12 terms depending on system size and method) and yields an extremely efficient method to avoid solving the full RPA yet achieving full RPA accuracy [14–16]. The SRPA is thus an ideal tool for large scale systematic investigations covering deformed [15] or large spherical clusters [14,16]. As it cooperates equally well with SAJM or PHJM, we will employ it also for the present case after a quick test of its applicability for our purposes.

2 Technical details

2.1 Handling the separable RPA

The SRPA [14,15] used in the present paper combines aspects of the vibrating potential model (or schematic model of RPA) [39–42] and the local RPA [13,25,34] expanding the residual interaction as a sum of separable terms. Due to the separable ansatz, the expensive RPA eigenvalue problem turns into a much simpler dispersion relation which is extremely helpful (if not compulsory) for systematic investigations of deformed and/or very large clusters. The force coefficients in the separable expansion are derived systematically and unambiguously from the given residual interaction. The RPA residual interaction is derived by second functional variation of the same energy-density functional that was used to compute the Kohn-Sham ground state. In practice, we are using here the energy-density functional of [43] for exchange and correlations.

There is some freedom in the choice of a basis set of input local operators. A good choice should embrace operators which couple to the surface plasmon, those which attach to the volume plasmon, and several more which account for polarization effects from higher states. A most efficient (*i.e.*, well converging) choice for the basis set of local operators in the expansion can be taken over from experience gained in the local RPA [25]. Similarly to [16], the set of 10 local $L = 1$ operators $f_p(\mathbf{r}) = (r/R)^p Y_{10}(\Theta)$ with $p = 1, 3, 5, 7$, and $f_q(\mathbf{r}) = j_1((q\pi/R)r)Y_{10}(\Theta)$ with q =2.0, 2.8, 3.6, 4.4, 5.2 and 6.0 is used. Here, $j_1((q\pi/R)r)$ is the spherical Bessel function, $Y_{10}(\Theta)$ is the dipole spherical harmonic, $R = r_s N_a^{1/3}$ is the jellium radius, and N_a is the number of atoms in a cluster. The radial parts of these basis operators (weighted with the ground state density) are peaked at different values of r, thus covering the surface as well as many slices of the interior of a cluster. This indicates how such a basis can embrace the coupling to the surface plasmon together with volume plasmon and further interior excitations. What remains is to check the convergence of the series when proceeding to new applications (new range of sizes, new materials, new potentials). Further details can be found in [14–16] whereby it is to be noted that these both presentations differ in details of the separable ansatz and in the actual handling of the dispersion relation. Here we recur to the version of [14,15] employing explicit particle-hole states from the underlying Kohn-Sham ground state. The above local operators are

used to derive self-consistently the operators of the residual interaction and these are used in the separable expansion (this differs from [16] where the expansion is done directly in terms of input local operators). The present scheme yields sufficient convergence with about four separable terms up to the largest clusters in the present investigation ($N_e = 440$) and for the chosen resolution (width). The enormous gain in efficiency can be easily read-off from the technical complexity: with SRPA we handle dispersion relations with matrices typically of rank 4 whereas a full RPA treatment of a cluster with $N_e = 440$ would invoke a diagonalization of 1000×1000 matrices.

2.2 Observables and their presentation

The SRPA in the present form leads to a spectrum of eigenstates with frequencies ω_j and associated $B(E1)_j$ values, *i.e.*, reduced probability of $E1$ transition from the ground state to the excited RPA state with the number j. All details of a calculation are visualized when plotting the discrete spectral states with their normalized oscillator strength $S(E1,\omega_j) = \omega_j B(E1)_j/m_1$ where $m_1 = \sum_j \omega_j B(E1)_j$ is the energy-weighted sum rule. This presentation shows in detail the amount of Landau fragmentation of the collective dipole strength over the neighboring dipole $1ph$ (particle-hole) states. Note that we use here frequencies ω_j synonymous with excitation energy and provide it in units of eV, which means that we implicitly use units with $\hbar = 1$.

Within PHJM the energy-weighted sum rule m_1 is modified with respect to the standard Thomas-Reiche-Kuhn expression by an amount which indicates the importance of nonlocal ionic effects. For sodium and potassium clusters these are negligible and only for Li one has a sizeable modification [17,18]. In the calculations presented below the RPA particle-hole basis was chosen large enough such that the sum rule is exhausted for all cases with an accuracy of 1–2%. Unfortunately, a detailed comparison of this sum rule with the experiment is not feasible at present because of the large uncertainties in the absolute measured cross-sections.

Actual experimental strength distributions look much smoother due to finite spectral resolution and, more importantly, due to thermal broadening of the resonance peaks (for a quantitative discussion see, *e.g.*, [47]). For comparison with data, we smoothed each (δ-like) distribution by a Lorentz function which yields a dipole strength distribution as $S_{E1}(\omega) = \sum_j S(E1,\omega_j)\rho(\omega - \omega_j)$ with $\rho(\omega - \omega_j) = (2\pi)^{-1}\dfrac{\Delta}{(\omega-\omega_j)^2 + (\Delta/2)^2}$. The value of the averaging parameter is $\Delta = 0.25$ eV which is tuned to roughly simulate the typical thermal broadening of the plasmon. The actual widths would, of course, vary with temperature and material. Since we do not aim at a detailed description of widths, we use here one average value to simplify matters. As will be seen in Figure 4, this average value provides appropriate results in all cases considered here.

Although Landau fragmentation leads to many details in the spectra, the main trends can well be characterized in terms of peak position and width. We deduce both properties from the smoothed strength distributions. The peak position is defined as the centroid energy analyzed in an interval which is centered at the peak and has a width of 1 eV. It needs to be determined in an iteration procedure. The corresponding width Γ is estimated within the following prescription [16]: the highest peak was picked and the farest occurrences of half the peak-height are determined above and below the peak. The width is then the energy difference of these two half-height points. This, as a rule, embraces the whole bump of the structured plasmon strength and, in the simplest case of a one-peak structure, reduces to a familiar full width at half maximum (FWHM). Finally, as a complementing global feature of the excitation spectrum, we evaluate the static dipole polarizability α which is related to inverse-energy-weighted sum rule: $\alpha = 2m_{-1} = 2\sum_j \omega_j^{-1} B(E1)_j$.

3 Results and discussion

3.1 Convergence of the SRPA expansion

The convergence of the SRPA results with the number of separable terms is demonstrated in Figure 1. As pointed out earlier [14–16], it is obvious that one separable term (the strictly separable RPA) is insufficient by far. The strength is too much blue shifted. But the results improve dramatically with each additional term in the expansion, such that good convergence is achieved with already four operators (with the radial dependence $(r/R)^p$ and $p = 1, 3, 5, 7$) leading, in fact, to the same result as in the case of 10 local operators. It is only the largest cluster in the sample, Na^+_{441}, for which one can spot tiny differences to the exact results (reached here certainly when using 10 separable terms [16]). This hints also that more terms may become necessary when stepping up to even larger clusters. It is also to be noted that a higher number of terms becomes necessary when aiming at a higher spectral resolution, see the tiny differences in the fully spectral presentation (up *versus* down bars in the two upper panels of Fig. 1). As a sideremark, the present SRPA technique achieves convergence for Na^+_{441} with four terms where the method of [16] would have required six terms for the same precision. The two methods differ in the way they employ the local operators in the separable ansatz. In [16] the residual interaction is parametrized directly in terms of these operators. In the method [14,15] which is exploited here the local operators are used as generators of the separable terms in the framework of the vibrating potential model [40,42]. This pre-processing leads naturally to a somewhat faster convergence.

Altogether, Figure 1 compares SRPA and full RPA (obtained without the separable approximation) results for Na^+_{21} and Na^+_{59}. The comparison proves again what had been shown extensively in previous works [14–16], namely that the separable expansion for Coulomb systems converges very well with respect to spectral properties in

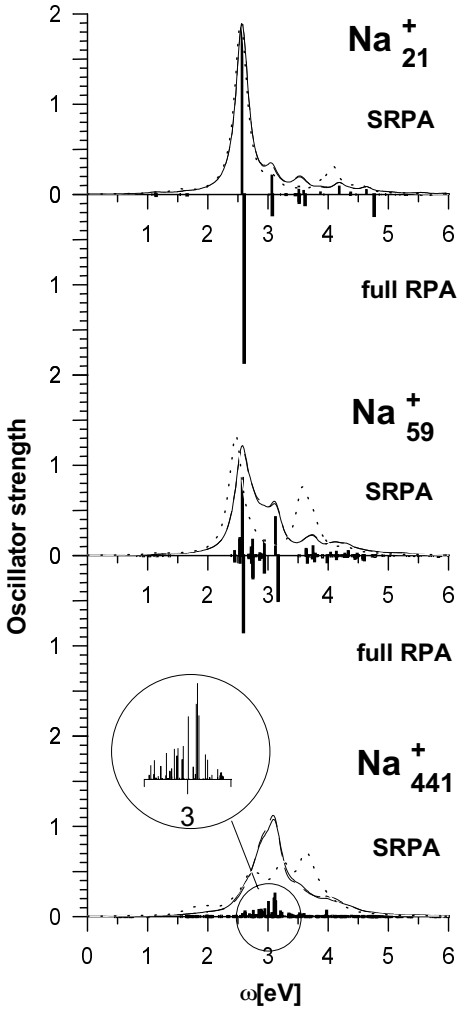

Fig. 1. The oscillator strength calculated in the framework of the SRPA (up) and full RPA (down) shown as bars (the latter is done for Na_{21}^+ and Na_{59}^+ only). The full line represents a smoothed strength distribution as averaged by a Lorentz function of width 0.25 eV. The length of the bars is rescaled by a factor 1/2.55 to fit the scale to the smoothed strength. The SRPA results are presented for several numbers of separable terms: dashed = 1, dash-dotted = 4, solid line = 10. The insert for Na_{441}^+ demonstrates the high density of RPA states covered by the dipole plasmon.

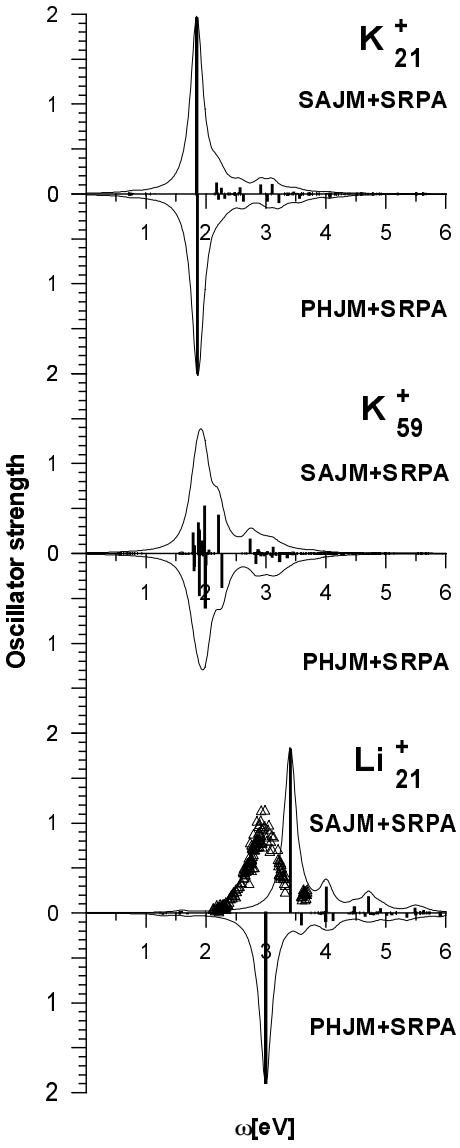

Fig. 2. The oscillator strength calculated in the framework of the SRPA with the SAJM (up) and PHJM (down) single-particle schemes. For Li_{21}^+ the photoabsorption experimental data (△) in $Å^2/N_e$ [10] are compared. The results are shown in the same fashion as in Figure 1.

general, and the dipole strength functions in particular. The actual number of separable terms needed is so small that SRPA delivers an extremely efficient scheme.

3.2 SAJM versus PHJM

Figure 2 compares dipole strengths calculated with SRPA using SAJM and PHJM for the ionic background. The cases K_{21}^+, K_{59}^+, and Li_{21}^+ are chosen as typical examples. The first two represent clusters with very weak nonlocal effects ($m_e^*/m_e = 1.02 \approx 1$), and with Landau fragmentation increasing with cluster size. The last example, Li_{21}^+, represents a cluster with strong nonlocal effects. One sees that for K_{21}^+ and K_{59}^+ both calculations, the SAJM+SRPA as well as the PHJM+SRPA, give almost identical results, especially for the smoothed dipole strength. This is not surprising since the nonlocal effects, which constitute the principle difference between the SAJM and PHJM, are not so large in potassium. We have checked similar results for Na clusters and find the same agreement between SAJM+SRPA and PHJM+SRPA as for K clusters. Nonlocal effects are thus negligible for computing the plasmon response in Na or K and the SAJM is quite sufficient for this purpose. In a similar fashion, one finds that a more detailed (not averaged) treatment of the ionic background in Na and K clusters can also be simplified by invoking

merely local pseudopotentials, as done *e.g.* in the cylindrically averaged pseudopotential scheme [54]. This positive experience has inspired further work to achieve a better fine-tuning of local pseudopotentials for simple metals, see [55] and references cited therein.

The lowest panel in Figure 2 shows the results for Li_{21}^+. Here we see large discrepancies between SAJM+SRPA and PHJM+SRPA. The PHJM+SRPA predicts a plasmon energy very close to the experimental data [10] while the SAJM+SRPA considerably overestimates the peak frequency of the plasmon resonance. This proves clearly the importance of nonlocal effects which are taken into account in the PHJM+SRPA.

3.3 Strength distributions

Figure 3 shows the dipole strength distributions for a broad selection of spherical, singly charged K, Na, and Li clusters. The results are compared with experimental data [6–10]. It is worth noting that these experimental data have been obtained at different temperatures: 350 K for K_9^+ and K_{21}^+ [6]; 600-800 K for K_{441}^+, Li_{139}^+ and Li_{441}^+ [8]; 560, 340, 310, 295 and 290 K for Na_9^+, Na_{21}^+, Na_{41}^+, Na_{59}^+ and Na_{93}^+, respectively [9]; 105 K for Li_9^+ and Li_{21}^+ [10]. An increase of the temperature causes a cluster dilatation and a corresponding redshift of the plasmon (see, for instance, [46,47]), which can be estimated as about 1% of the plasmon energy per 100 K [7,48]. We have employed the Wigner-Seitz radii at room temperature. The temperature effect on the plasmon position can thus reach 5% in the worst case, but stays generally below 2%. Moreover, the bulk melting temperature is $T_b = 336$, 371 and 452 K for K, Na and Li, respectively. So, one may assume that at least clusters K_{441}^+, Li_{139}^+ and Li_{441}^+ have been measured in a liquid-like phase.

It worth noting that both the SAJM and PHJM, though taking into account some core electron effects, are, nevertheless, based on the jellium approximation. So we do not pretend to describe the photoabsorption experimental data in the cases where the detailed arrangement of ions is particularly essential (for example, the fragmentation of the dipole strength in Na_9^+ observed at low temperature, 105 K [49]) and, to be consistent, will compare our results mainly with high-temperature photoabsorption data where available (see Refs. above). The single exception will be the case of small Li clusters where we recur to low-temperature experimental data because we could not find any other measurements of the dipole response for these clusters at higher temperatures.

The computed strength distributions in Figure 3 agree generally well with the experimental data for Na and K clusters, and for the small Li clusters. They reproduce even some details as the shoulder above the plasmon peak in case of Na_{21}^+, Na_{59}^+ and Li_{21}^+. In Na clusters the most noticeable deviation from the experiment takes place in Na_{41}^+ where we got the double-peak plasmon instead of one-peak profile observed experimentally. The SAJM calculations predict for this cluster the octupole deformation in the ground state [50] while in the present paper Na_{41}^+ is supposed to be spherical. Most probably, this is the main reason of the discrepancy. The other deviations from the experiment are of minor character: the calculated plasmon energies are slightly redshifted by 0.1–0.15 eV in K_9^+, K_{21}^+ and Na_{21}^+ and blueshifted by about the same value in K_{441}^+. The deviation for K_{441}^+ could be partially attributed to (a) the high temperature of 600–800 K in the experiments which would favor a redshift and (b) core-polarization effects which are small but can cause a few percent redshift in large clusters. Generally, good agreement of the calculations with the experimental data for such a wide group of clusters shows that the SAJM+SRPA and PHJM+SRPA provide quite reliable models.

While small lithium clusters are well-described, there are substantial deviations for the large lithium clusters Li_{139}^+ and Li_{441}^+, where the PHJM+SRPA calculations yield a blue-shift by ≈ 0.5 eV as compared with the experimental plasmon frequency. Besides, for Li_{441}^+ the width is greatly underestimated. These results are similar to those found in reference [18] when using the full pseudopotentials (see Fig. 6 of that reference), and thus confirm that the accuracy of the present pseudo-Hamiltonian parameterization is similar to that of the full pseudopotential. Additionally, this shows again that the good agreement with the experiment for large Li clusters obtained in the first PHJM calculations of reference [17] was rather spurious and due to an incorrect parameterization of the atomic pseudo-Hamiltonian. This sensitivity of the pseudo-Hamiltonian parameterization is more important the bigger the cluster (in big clusters the contribution of the kinetic energy to the restoring force and, therefore, the influence of the effective mass is more essential) and yields substantial differences in the bulk limit [23]. In small Li clusters the results are much more stable. In fact, as is seen in Figure 3, the new parameterization gives a striking agreement with the experiments for Li_9^+ and Li_{21}^+.

The failure of the PHJM+SRPA in large Li clusters could be attributed to different effects which are not included in this model. We mention the following as important sources of discrepancy:

a) large temperatures in the photoabsorption experiments for big Li clusters which would induce a redshift in the energy and increase the width;
b) effects of the cluster ionic array on the electronic properties, similarly to the band structure in bulk Li [51,52], which are washed out by the spatial average of PHJM. However, the photoabsorption measurements for large clusters have been performed at a high temperature, 600–800 K, and so these clusters were in the liquid-like phase, which could suppress band structure effects;
c) the present PH parameterization [22], although an improvement compared to the previous one [37], is perhaps still insufficient to describe correctly the dynamics of valence electrons in large Li clusters. We remind that the PH parameterizations [22,37] were tuned to reproduce static properties. At the same time, electronic dynamics is also sensitive to details of pseudopotentials and corresponding pseudo-Hamiltonians;

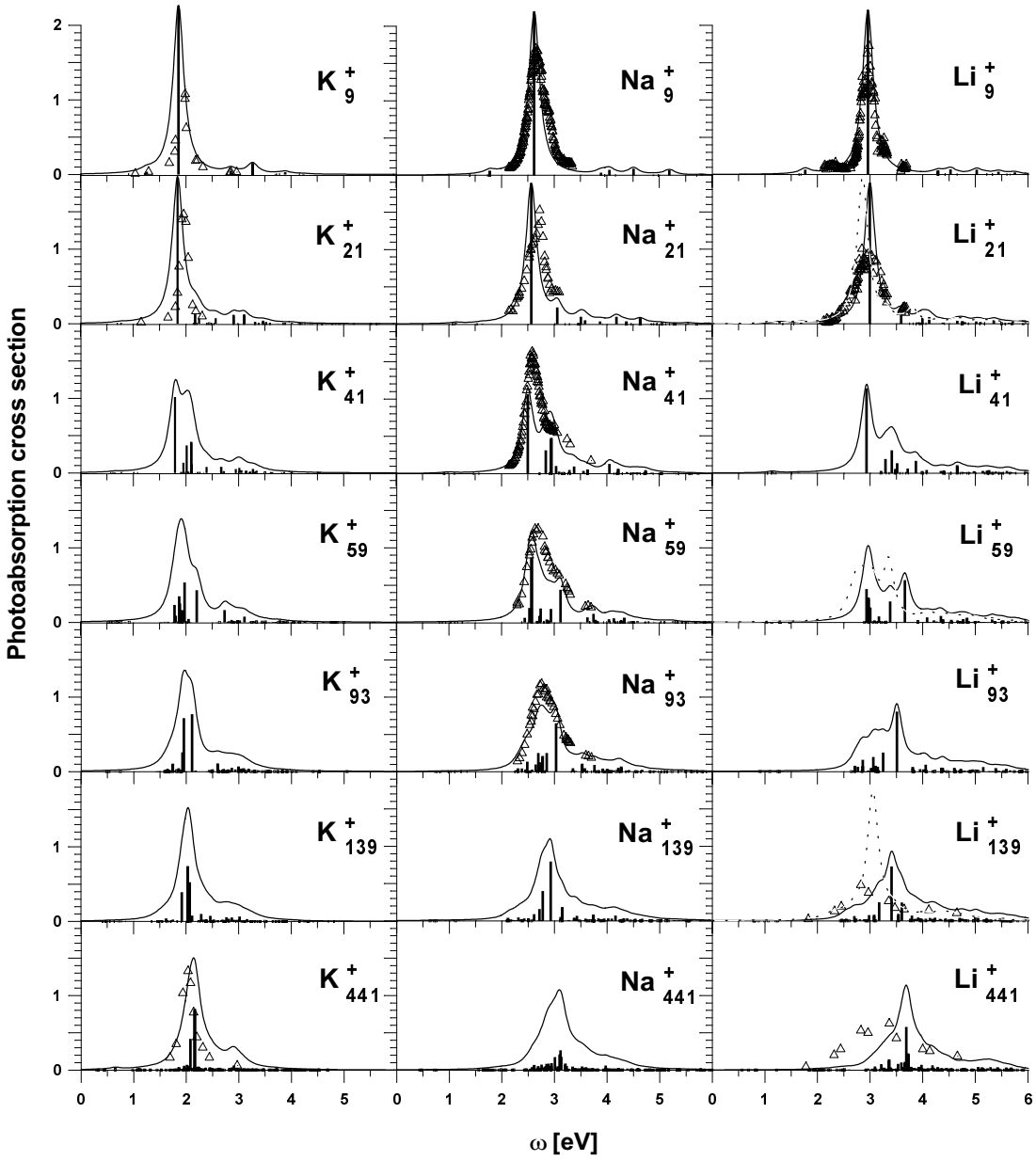

Fig. 3. The SRPA oscillator strength compared with the photoabsorption data (△) in $Å^2/N_e$ for K, Na and Li clusters (K_9^+, K_{21}^+ [6], K_{441}^+, Li_{139}^+, Li_{441}^+ [8], $Na_9^+ - Na_{93}^+$ [9] and Li_9^+, Li_{21}^+ [10]). The K and Na clusters use the SAJM background whereas Li employs the PHJM. The dotted line for Li_{21}^+, Li_{59}^+ and Li_{139}^+ represents the PHJM+SRPA results obtained with the PH parameterization from reference [37]. The results are given in the same fashion as in Figure 1. The experimental data for K are decreased by the factor 2 to provide an appropriate scale.

d) a *direct* contribution of dynamical core-polarization effects to the dielectric response. In the present model, we treat properly the static contribution while the dynamical one is incorporated only through the effective mass, which could be insufficient for Li clusters. It was shown recently for the case of Ag clusters that dynamical core polarization can be treated explicitly and that it plays a crucial role for the dielectric response, leading to a considerable decrease of the plasmon frequency [44]. In general, it was found that the stronger the nonlocal contribution of the ionic core polarization and the bigger the cluster, the larger the redshift of the plasmon frequency. A similar readshift may be expected for large Li clusters because these, unlike K and Na, exhibit strong nonlocal ion-core effects already in the ground state [17,18,20–22].

In any case, large Li clusters need further careful fine-tuning of nolocality properties and ionic background models in order to achieve the good agreement seen for Na and K clusters.

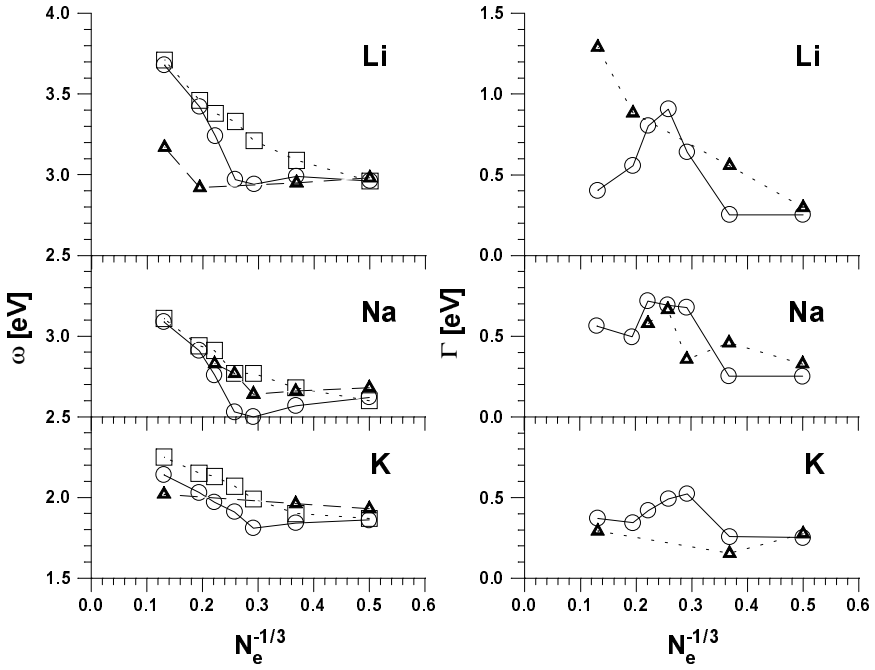

Fig. 4. Plasmon frequencies (left) and widths (right) *versus* $N_e^{-1/3}$. For the frequencies we show energy centroids (boxes) as well as positions of highest peaks (circles). The SRPA results are compared with experimental data (triangles) [6–10].

3.4 Trends

Figure 4 shows the trends with $N_e^{-1/3}$ for the plasmon frequencies ω and widths Γ which were extracted from the strength distributions as explained at the end of Section 2.2. We had seen in Figure 3 that the strengths in many clusters have a rather structured form which is not easily characterized by one peak position. Therefore, we provide in Figure 4 also the frequencies of highest peaks. The difference between plasmon and highest peak frequencies allows to estimate the uncertainty in a peak assignment caused by the fragmentation pattern.

All trends from the SRPA calculations in Figure 4 look quite similar for K, Na, and Li clusters. The frequencies decrease from a bulk limit (close to the Mie value) and for decreasing size as $N_e^{-1/3}$. However, at $N_e \approx 50$ this trend levels off or even turns into a slight increase. The linear decrease is due to the spill-out of the electron cloud [34]. The spill-out is a surface effect and remains about independent of system size (for not too small clusters), but the ratio of surface to volume increases with decreasing size which then explains the observed trend. For small clusters, however, the quantization of the $1ph$ states comes up as a process which limits the resonance position from below thereby stopping the linearly decreasing trend.

The widths show also similar trends for K, Na and Li clusters. For small clusters, there is a vacuum of $1ph$ states at resonance frequency which leads to very narrow peaks, representing here basically the imposed background width. Landau fragmentation sets on for $N_e \gtrsim 40$ where we see a strong increase in width. It is interesting to note that this increase in width is accompanied by an increasing difference between the two definitions of a peak (see left panel of Fig. 4). For very large clusters, one expects again a decrease [16,41]. This trend, however, becomes manifest only for cluster sizes $N_e > 1000$ and requires investigations which go up to much larger sizes, as *e.g.* in [16,21]. It is worth mentioning that the observed widths come in any case predominantly from Landau fragmentation. Large clusters show a sizeable fragmentation in spite of the spherical shape, whereas small clusters require thermal averages in ensembles containing octupole deformed clusters for which Landau damping is activated by symmetry breaking [47].

Comparing with the experimental data in Figure 4, we see that the trends of widths and frequencies with the material are essentially reproduced. The calculations confirm the general increase of the plasmon width from K to Li, discussed in many papers. This increase in our calculations is not so strong as in experiment [8] and in some RPA calculations (see Fig. 16 for K_{440}, Na_{440} and Li_{440} in [35]). The difference with reference [35] can be partly explained by the fact that we use here more realistic single-particle schemes where the decrease of the width of the single-particle potential from K to Li is partly compensated by the increase of the potential depth (in Ref. [35] a square potential well with three different potential widths, $2r_sN^{1/3}$, was exploited). The discrepancy with experimental trends is mainly caused by the too small calculated width in Li^+_{441} (see above the discussion for large Li clusters). Looking at the trends with $N_e^{-1/3}$ for fixed material, we see that they come out best for Na clusters. For K clusters the agreement is also good. However, the supply of measured clusters is too small for a detailed comparison, specially in region of medium sizes. The case of Li is worse. As already seen in Figure 3 and extensively discussed above, the calculations for large Li clusters produce too high peak frequencies and too low widths.

As complementing information, we show in Figure 5 the static dipole polarizabilities α calculated within the SRPA. They demonstrate an expected general decrease with size, based on the decreasing importance of the

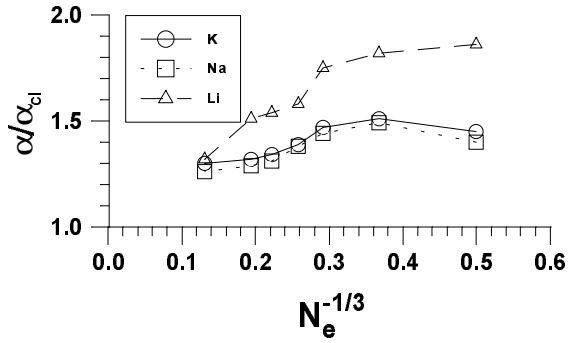

Fig. 5. SRPA results for the static dipole polarizabilities α (in units of $\alpha_{cl} = r_s^3 N_a$) *versus* $N_e^{-1/3}$ (see text).

electronic spill-out. The kink at $Na_{41}^+ - Na_{59}^+$ is connected with the corresponding kink in plasmon energies discussed above. The normalized values α/α_{cl} in Li clusters are considerably larger than in K and Na due to larger spill-out in Li clusters which, in turn, is caused by the large non-local effects.

3.5 Details of the Landau fragmentation

We have seen in the detailed Figure 3 and in the trends in Figure 4 that the Landau damping for spherical clusters changes dramatically from small clusters, $N_e \lesssim 20$, to larger clusters, $N_e \gtrsim 40$. This feature is related to shell structure, as has been discussed earlier [12,25]. The surface plasmon resonance lies in a "vacuum" of $1ph$ states for small clusters. But the $1ph$ energies shrink $\propto N_e^{-1/3}$ and interfere necessarily with the resonance at some point, which comes typically around $N_e \sim 40$. From that point on, one has always a large level density near the resonance which leads to a substantial Landau damping. The level density increases with size and so increases the width. But a further mechanism comes into play for even larger clusters: the coupling between the resonance and $1ph$ states fades away due to increasing mismatch of momenta. This leads to a decrease of the plasmon width $\propto N_e^{-1/3}$, estimated analytically in the wall formula [41] and tested in extensive SRPA calculation [16].

The interplay between plasmon position and dipole $1ph$ states (*i.e.* states taking place without the residual interaction) for the present samples is visualized in Figure 6. Here we have distinguished the $1ph$ dipole transitions according to their shell spacing $\Delta\mathcal{N} = 1, 3, 5, ...$, where $\mathcal{N} = 2(n-1) + l$ is the principle shell quantum number with n and l being the number of the nodes and orbital momentum of the single-particle wave function. These $1ph$ configurations represent the unperturbed dipole states which constitute the excitation spectrum if the residual interaction is neglected. One sees in Figure 6 that the spectra are bunched in groups of $\Delta\mathcal{N}$, with well-separated gaps for small clusters and small $\Delta\mathcal{N}$ and with a tendency to overlap for larger systems or larger $\Delta\mathcal{N}$. The gaps are better separated for small clusters since the single-particle potential there comes close to a harmonic oscillator shape. In larger clusters, on the other hand, the single-particle potential resembles more a square well which produces less bunching of the single particle states. The corresponding decrease of shell gaps with increasing the size is a common feature of saturating Fermion systems, *i.e.* systems which approach a constant density, see, *e.g.*, reference [56].

The dipole plasmon is mainly generated by the $\Delta\mathcal{N} = 1$ configurations first placed at 0.5–1.5 eV. Due to the residual interaction, the $\Delta\mathcal{N} = 1$ oscillator strength is mixed and blueshifted to form the plasmon at the appropriate energy which is indicated by arrows in Figure 6. The shift increases strongly with system size due to the long range of the Coulomb forces such that the emerging plasmon position changes very little with electron number (this is different, *e.g.*, from the case of the nuclear giant resonances generated from a short-range interaction, see [25]). The large shift now places the plasmon far away from the original $\Delta\mathcal{N} = 1$ shell. In small clusters the plasmon lies in the wide gap between $\Delta\mathcal{N} = 1$ and 3 and remains unperturbed as a clean collective peak. This is ideally realized in the cases $N_e = 8$. The $N_e = 20$ in Figure 6 represents already a limiting stage where the resonance approaches the next bunch of the $\Delta\mathcal{N} = 3$ states. It does this in similar fashion for all three materials. This leads to the onset of fragmentation for this cluster sizes, as observed in Figure 3. The medium size clusters (the case $N_e = 58$ in Fig. 6) find the plasmon already fully interfering with the $\Delta\mathcal{N} = 3$ bunch which corresponds nicely to the sizeable Landau fragmentation seen in Figures 3 and 4. The plasmon runs deeper into a swamp of $1ph$ states for larger clusters, as nicely seen for the case $N_e = 440$ in Figure 6. This leads to the general trend of increasing width which is, however, overlaid by strong fluctuations. These fluctuations are related to the fluctuations in level density at resonance position which can also be read off from Figure 6. For very large clusters with $N_e > 1000$ the level density is so smooth that fluctuations shrink and the resonance develops into one broad unstructured peak [16]. This is, on the other hand, the point where the width starts to shrink with a size (as reviewed above). We want to remark that these general trends are the same for the materials shown in Figure 6. They are, in fact, valid for all simple metals.

4 Summary

Systematic investigations of the dipole plasmon for K, Na and Li clusters have been performed in a wide range of sizes for which experimental results are available. The ionic structure was treated within the pseudo-Hamiltonian jellium model (PHJM), that takes into account possible nonlocal effects on the valence electrons. These are specially important in Li. For the Na and K cases, where nonlocal effects are negligible, we have explicitly shown that the PHJM is equivalent to the structure-averaged jellium model (SAJM) and have used this for the systematic calculations. The dipole optical response was calculated within the separable random-phase-approximation

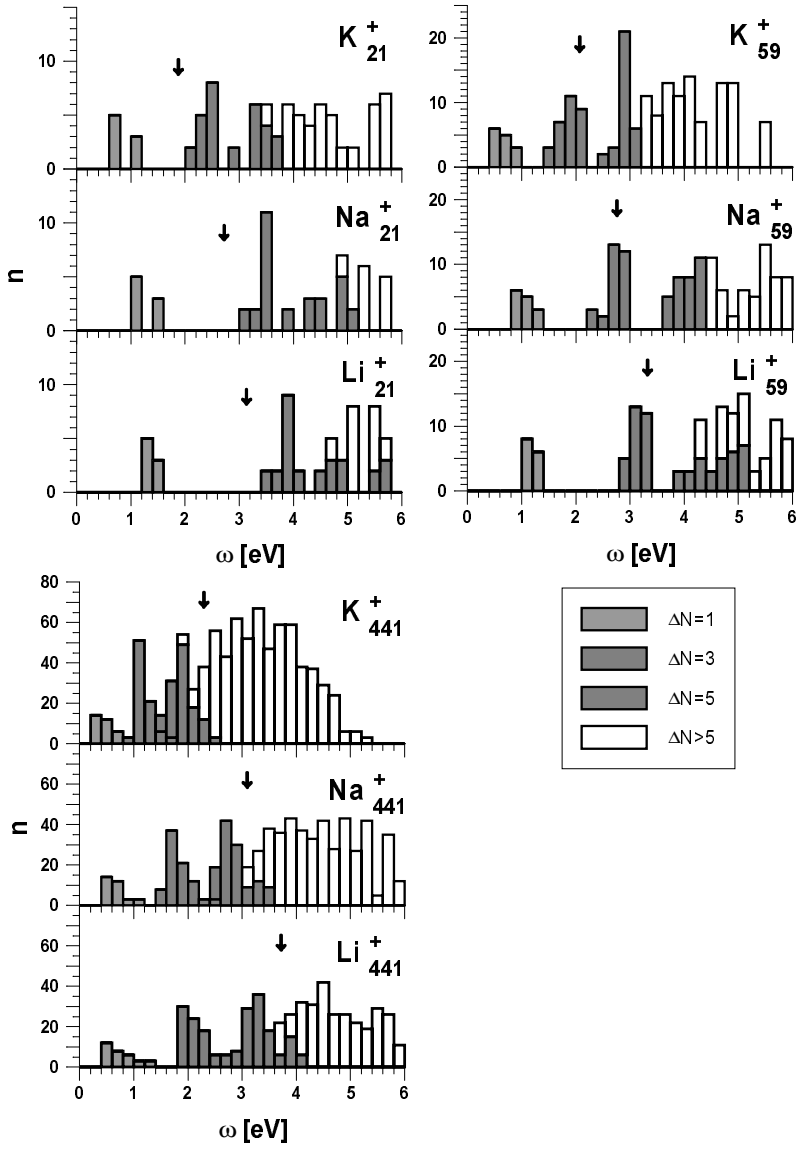

Fig. 6. Histograms showing, as a function of the energy, the number of dipole particle-hole configurations corresponding to $\Delta\mathcal{N} = 1$ (light dotted bricks), $\Delta\mathcal{N} = 3$ (dashed bricks), $\Delta\mathcal{N} = 5$ (dark dotted bricks) and $\Delta\mathcal{N} \geq 7$ (unfilled bricks) dipole transitions in small, medium and large K, Na and Li clusters. $\mathcal{N}$ is the principal shell quantum number. The arrows mark centroid energies of the plasmon. Note the different scales used for small, medium and large clusters.

(SRPA), which is actually an RPA using a separable expansion for the residual interaction. The separable expansion of the SRPA converges rapidly such that a sum of four separable terms was sufficient for the clusters studied here. This rapid convergence reduces drastically the computational effort, yielding at the same time the full accuracy of RPA methods.

The results from SAJM+SRPA and PHJM+SRPA are in good agreement with most of the available experimental data. The SAJM+SRPA (relying on folding with local pseudopotentials) turned out to be sufficient for K and Na clusters whereas the nonlocal effects incorporated in the PHJM+SRPA are required to describe properly Li clusters. The calculations reproduce the correct trends of the plasmon frequencies and widths with cluster size. These trends with size are very similar for K, Na, and Li clusters. The trends with changing material, namely an increase in plasmon frequency and width from K over Na to Li, are also reproduced by the calculations. The leading role of the Landau damping for the plasmon width in medium and large clusters was analyzed in detail, showing also that a substantial fine structure remains in the spectra of medium sized clusters.

In spite of the general success of the models, we ought to point out that still a large discrepancy remains for the large Li clusters Li^+_{139} and Li^+_{441}: the calculations overestimate the plasmon frequency and underestimate the width. There are several conceivable reasons for that defect (thermal expansion, missing band structure, insufficiencies in the pseudopotential, dynamical core-polarization) which yet need to be checked in detail.

We are grateful to C. Ellert and H. Haberland for communicating the experimental results for small Li clusters before publication. The work was partly supported by INTAS, grant 0151 (V.O.N.), and by the Spanish DGES, grant PB95-0492 (Ll.S.).

References

1. W.D. Knight, K. Clemenger, W.A. de Heer, W.A. Saunders, M.Y. Chou, M.L. Cohen, Phys. Rev. Lett. **52**, 2141 (1984).
2. W. Ekardt, Phys. Rev. Lett. **52**, 1925 (1984).
3. D.E. Beck, Phys. Rev. B **30**, 6935 (1984).
4. K. Selby, M. Vollmer, J. Masui, V. Kresin, W.A. de Heer, W.D. Knight, Phys. Rev. B **40**, 5417 (1989).
5. J. Borggreen, P. Chowdhury, N. Kebaili, L. Lundsberg-Nielsen, K. Lützenkirchen, M.B. Nielsen, J. Pedersen, H.D. Rasmussen, Phys. Rev. B **48**, 17507 (1993); P. Meibom, M. Ostergård, J. Borggreen, S. Bjornholm, H.D. Rasmussen, Z. Phys. D **40**, 258 (1997).
6. C. Bréchignac, Ph. Cahuzac, J. Leygnier, J. Weiner, J. Chem. Phys. **90**, 1492 (1989); C. Bréchignac, Ph. Cahuzac, F. Carlier, M. de Frutos, J. Leygnier, J. Chem. Phys. **93**, 7449 (1990).
7. C. Bréchignac, Ph. Cahuzac, N. Kebaili, J. Leygnier, A. Sarfati, Phys. Rev. Lett. **68**, 3916 (1992).
8. C. Bréchignac, Ph. Cahuzac, J. Leygnier, A. Sarfati, Phys. Rev. Lett. **70**, 2036 (1993).
9. Th. Reiners, Ch. Ellert, M. Schmidt, H. Haberland, Phys. Rev. Lett. **74**, 1558 (1995).
10. C. Ellert, H. Haberland (private communication).
11. J.M. Pacheco, W. Ekardt, Ann. Phys. (Leipzig) **1**, 254 (1992).
12. C. Yannouleas, E. Vigezzi, R.A. Broglia, Phys. Rev. B **47**, 9849 (1993).
13. P.-G. Reinhard, M. Brack, O. Genzken, Phys. Rev. A **41**, 5568 (1990).
14. V.O. Nesterenko, W. Kleinig, V.V. Gudkov, N. Lo Iudice, J. Kvasil, Phys. Rev. A **56**, 607 (1997).
15. V.O. Nesterenko, W. Kleinig, *Proc. Intern. Symp. Similarities and Differences between Atomic Nuclei and Clusters* (Tsukuba, Japan, 1997), *AIP Conference Proceedings 416*, edited by Y. Abe, I. Arai, S.M. Lee, K. Yanaba (Woodbury, New York, 1998), p. 77.
16. J. Babst, P.-G. Reinhard, Z. Phys. D **42**, 209 (1997).
17. Ll. Serra, G.B. Bachelet, N. van Giai, E. Lipparini, Phys. Rev. B **48**, 14708 (1993).
18. F. Alasia, Ll. Serra, R.A. Broglia, N. van Giai, E. Lipparini, H.E. Roman, Phys. Rev. B **52**, 8488 (1995).
19. Ll. Serra, E. Lipparini, N. Van Giai, Europhys. Lett. **29**, 445 (1995).
20. S.A. Blundell, C. Guet, Z. Phys. D **33**, 153 (1995).
21. F. Catara, Ph. Chomaz, N. Van Giai, Z. Phys. D **33**, 219 (1995).
22. J. Lermé, Phys. Rev. B **54**, 14158 (1996).
23. E. Lipparini, N. Van Giai, Ll. Serra, J. Phys.-Cond. **7**, 4467 (1995).
24. B. Montag, P.-G. Reinhard, J. Meyer, Z. Phys. D **32**, 125 (1994).
25. P.-G. Reinhard, O. Genzken, M. Brack, Ann. Phys. (Leipzig) **5**, 576 (1996).
26. A. Rubio, Ll. Serra, Z. Phys. D **26**, S118 (1993).
27. F. Calvayrac, E. Suraud, P.-G. Reinhard, Phys. Rev. B **52**, R17056 (1995).
28. K. Yabana, G.F. Bertsch, Phys. Rev. B **54**, 4484 (1996).
29. C. Guet, W.R. Johnson, Phys. Rev. B **45**, 11283 (1992).
30. E. Lipparini, Ll. Serra, K. Takayangi, Phys. Rev. B **49**, 16733 (1994).
31. M. Koskinen, M. Manninen, P.O. Lipas, Phys. Rev. B **49**, 8418 (1994).
32. V. Bonacic-Koutecky, P. Fantucci, J. Koutecky, Chem. Rev. **91**, 1035 (1991).
33. W.A. de Heer, Rev. Mod. Phys. **65**, 611 (1993).
34. M. Brack, Rev. Mod. Phys. **65**, 677 (1993).
35. C. Brechignac, J.P. Connerade, J. Phys. B **27**, 3795 (1994).
36. A. Rubio, J.A. Alonso, X. Blase, S.G. Louie, Int. J. Mod. Phys. B (to be published, 1997).
37. G.B. Bachelet, D.M. Ceperley, M. Chiochetti, Phys. Rev. Lett. **62**, 2088 (1989).
38. A. Rubio, L.C. Balbas, J.A. Alonso, Z. Phys. D **19**, 93 (1991).
39. D.J. Rowe, *Nuclear Collective Motion* (Methuen, London, 1970), Chaps. 4 and 14–16.
40. E. Lipparini, S. Stringari, Z. Phys. D **18**, 193 (1991).
41. C. Yannouleas, R.A. Broglia, Ann. Phys. **217**, 105 (1992).
42. V.O. Nesterenko, W. Kleinig, V.V. Gudkov, Z. Phys. D **34**, 271 (1995).
43. O. Gunnarson, B.I. Lundqvist, Phys. Rev. B **13**, 4274 (1976).
44. Ll. Serra, A. Rubio, Phys. Rev. Lett. **78**, 1428 (1997); Czech. J. Phys. (1998) in press (*Proceedings of the Int. Symposium Atomic nuclei and Metallic clusters*, Prague, Czech Republic, 1997).
45. A. Hinterman, M. Manninen, Phys. Rev. B **27**, 7262 (1983).
46. A. Bulgak, C. Lewenkopf, Europhys. Lett. **31**, 519 (1995).
47. B. Montag, P.-G. Reinhard, Phys. Rev. B **51**, 14686 (1995).
48. *Hand Book of Chemistry and Physics Particles* (Chemical Rubber, Cleveland, 1967), p. 56.
49. Ch. Ellert, M. Schmidt, Th. Reiners, H. Haberland, Z. Phys. D **39**, 317 (1997).
50. Th. Hirschmann, B. Montag, J. Meyer, Z. Phys. D **37**, 63 (1996).
51. K. Sturm, Adv. Phys. **31**, 1 (1982).
52. F. Aryasetiawan, K. Karlsson, Phys. Rev. Lett. **73**, 1679 (1994).
53. Ch. Ellert, M. Schmidt, Ch. Schmidt, Th. Reiners, H. Haberland, Phys. Rev. Lett. **75**, 1731 (1995).
54. B. Montag, P.-G. Reinhard, Z. Phys. D **33**, 265 (1995).
55. S. Kümmel, M. Brack, P.-G. Reinhard, Phys. Rev. B (to be published, 1998).
56. H. Nishioka, K. Hansen, B.R. Mottelson, Phys. Rev. B **42**, 9377 (1990)